




Weak and strong coupling of photons and excitons in planar meso-cavities

ALEXEY V. BELONOVSKI,¹ IAROSLAV V. LEVITSKII,^{2,3} KONSTANTIN M. MOROZOV,² GALIA POZINA,^{4,*}  AND MIKHAIL A. KALITEEVSKI^{1,2,3}

¹St. Petersburg Academic University, Khlopina 8/3, 194021 St. Petersburg, Russia

²ITMO University, Kronverkskiy pr. 49, 197101 St. Petersburg, Russia

³Ioffe Institute, Politekhnicheskaya ul. 26, 194021 St. Petersburg, Russia

⁴Department of Physics, Chemistry and Biology (IFM), Linköping University, S-581 83 Linköping, Sweden

*galia.pozina@liu.se

Abstract: The interaction of an exciton and cavity modes is considered in planar meso-cavities, which have lateral sizes corresponding to few wavelengths. In meso-cavities, the frequency interval between the optical modes is comparable or smaller than the value of the Rabi splitting between the exciton and the optical modes. The Hamiltonian of the interaction between the exciton and the cavity modes is constructed, and it is shown that such an interaction between the cavity modes and the exciton can occur both in weak and in strong coupling regimes. The latter case can be accompanied by a pronounced splitting of the emission peaks as shown for modelled meso-cavities of triangular, square and hexagonal shapes, where it is demonstrated that Q-factors for the adjacent cavity modes as well as the strength of interaction with excitons can differ by few orders of magnitude.

© 2020 Optical Society of America under the terms of the [OSA Open Access Publishing Agreement](#)

1. Introduction

The study of semiconductor microcavities began with the pioneering work of Weisbuch *et al.*, in 1992 [1], where splitting was observed in the absorption and reflection spectra of excitons in the quantum wells placed in the centre of a resonant epitaxially grown planar microcavity. This splitting was interpreted as the vacuum Rabi splitting of the exciton resonance. Over the past three decades, these findings have led to extensive research in the field of strong light-matter coupling in semiconductor microcavities [2–14], which has resulted in the observation of a number of fascinating effects, including the demonstration of a polariton laser [14–15]. Strong coupling regime between exciton and cavity modes can occur in cylindrical [7,16] and spherical microcavities [17,18], two-dimensional lattices and other types of resonators. For all cases, it is essential that the characteristic size of the cavity corresponds to a fraction of the wavelength in order to ensure a large energy interval between the cavity modes. In such situation, only one or two cavity modes will interact with the exciton and the Rabi splitting will be smaller than the separation between the cavity modes, which makes it possible to observe the strong coupling regime. Achieving these conditions becomes more challenging for microcavities based on wide-band semiconductors, such as III-nitrides or ZnO, where the Rabi splitting is relatively large, while the Bohr radius and exciton emission wavelength are reduced in comparison with, for example, GaAs. However, the fabrication of smaller cavities suitable for UV nanophotonic applications is a technological bottleneck. Therefore, it is crucial to study larger resonators, the so-called meso-cavities, with a characteristic size corresponding to dozens of wavelengths.

We note that there is a certain parallelism between meso-cavities, which we consider in this work, and mesoscopic systems with corresponding effects for electrons. For an electronic system, when the coherence length of electrons becomes comparable with the characteristic scale of the system, a number of fascinating effects can arise, for example, weak localization, quantum

corrections to conductivity, quantum chaos, Aharonov–Bohm effect [19–22]. In meso-cavities with a size that provides an interval between energy levels and is comparable with the strength of the interaction between the photon and exciton modes (Rabi splitting), interesting effects of a similar origin can also be expected.

Thus, the purpose of this work is to consider theoretically the interaction of the exciton and the cavity modes in meso-resonators of various geometrical shapes for the two-dimensional (2D) case. In this situation, although the energy interval between the cavity modes is smaller than the Rabi splitting, the quality (Q) factors of the neighbouring modes and the strength of the interaction between the cavity mode and the exciton can differ substantially, which, as shown, can lead to peculiar effects related to the interaction of resonator modes and excitons. We will analyse the spectrum of modes for the 2D triangular, square, hexagonal, and circular cavities.

The choice of the specific shapes considered here is justified by technological achievements in the fabrication of planar microstructures based on different semiconductors. For example, triangular microcavities were obtained by etching InGaAsP semiconductor alloys [23]; circular, hexagonal and various rectangular microstructures based on GaN and ZnO were produced either by etching [24–26] or by the bottom-up growth approach using selective area epitaxy [27–29]. The Hamiltonian of the interaction between exciton and resonator modes will be constructed for aforementioned 2D meso-cavities, and the Hopfield coefficients characterizing the contribution of the exciton and cavity to polaritonic modes will be calculated.

2. Theory

We have analysed the polaritonic mode structure applying the following approach: the Hamiltonian for a system consisting of exciton and photon modes can be simplified by using the rotating wave approximation, i.e. under the assumption that energy conservation is preserved during the interaction.

In the case of the exciton Hamiltonian, we will exploit the second quantized form and field operators in order to work in a consistent mathematical framework.

The total Hamiltonian reads [15]:

$$\mathcal{H} = \hbar\omega_0\hat{x}^+\hat{x} + \sum_k \hbar\omega_k\hat{c}_k^+\hat{c}_k + \sum_k \hbar(g_k\hat{c}_k\hat{x}^+ + g_k^*\hat{c}_k^+\hat{x}), \quad (1)$$

where \hat{x}^+ , \hat{c}_k^+ are the operators of creation of exciton and photons, respectively, \hat{x} , \hat{c}_k are the operators of annihilation of exciton and photons, respectively, ω_0 is the exciton frequency, ω_k are the frequencies of cavity modes, g_k are constants describing the strength of the interaction of the exciton with the optical modes. The Hamiltonian of the interaction (Eq. (1)) in the matrix form reads as:

$$\mathcal{H} = \hbar[\hat{x}^+ \hat{c}_1^+ \hat{c}_2^+ \cdots \hat{c}_N^+] \cdot \begin{bmatrix} \omega_0 & g_1 & g_2 & \cdots & g_N \\ g_1^* & \omega_1 & 0 & \cdots & 0 \\ g_2^* & 0 & \omega_2 & \cdots & 0 \\ \vdots & \vdots & \vdots & \ddots & \vdots \\ g_N^* & 0 & 0 & \cdots & \omega_N \end{bmatrix} \cdot \begin{bmatrix} \hat{x} \\ \hat{c}_1 \\ \hat{c}_2 \\ \vdots \\ \hat{c}_N \end{bmatrix} = \hbar\hat{C}^+ W \hat{C}, \quad (2)$$

where C^+ is a row, which is made up of operators of creation, C is a column, which is made up of operators of annihilation, W is a square matrix, which consists of energies of the system and constants g_k .

The square matrix W is Hermitian; therefore, its diagonalization is possible with the help of a unitary transformation [30]:

$$A^{-1}WA = \lambda, \quad (3)$$

where A is a unitary matrix whose columns contain the eigenvectors of the matrix W , λ is the diagonal matrix whose elements are the eigenvalues of the matrix W . Inserting this result in Eq. (2) leads to:

$$\mathcal{H} = \hbar \cdot \hat{C}^+ A \cdot \lambda \cdot A^{-1} \hat{C}. \quad (4)$$

The expression $\hat{C}^+ A$ gives a new form of the operators of creation in the mixed system «exciton + modes». $A^{-1} \hat{C}$ is a new form of operators of annihilation. Consider this expression:

$$\begin{aligned} \hat{C}^+ A = [\hat{x}^+ \hat{c}_1^+ \hat{c}_2^+ \cdots \hat{c}_N^+] \begin{bmatrix} a_{00} & a_{01} & a_{02} & \cdots & a_{0N} \\ a_{10} & a_{11} & a_{12} & \cdots & a_{1N} \\ a_{20} & a_{21} & a_{22} & \cdots & a_{2N} \\ \vdots & \vdots & \vdots & \ddots & \vdots \\ a_{N0} & a_{N1} & a_{N2} & \cdots & a_{NN} \end{bmatrix} &= [\hat{x}^+ a_{00} + \sum_{j=1}^N \hat{c}_j^+ a_{j0}; \hat{x}^+ a_{01} \\ &+ \sum_{j=1}^N \hat{c}_j^+ a_{j1}; \cdots; \hat{x}^+ a_{0N} + \sum_{j=1}^N \hat{c}_j^+ a_{jN}] = [\hat{\rho}_0^+ \hat{\rho}_1^+ \cdots \hat{\rho}_N^+] = \hat{P}^+, \end{aligned} \quad (5)$$

where $\hat{\rho}_k^+ = \hat{x}^+ a_{0k} + \sum_{j=1}^N \hat{c}_j^+ a_{jk}$ is a new form of operator of creation. \hat{P}^+ is a row made up of the new operators of creation. Similar transformations can be carried out with another expression $A^{-1} \hat{C} = \hat{P}$, where \hat{P} is a column made up of operators of annihilation.

Eigenvalues λ_i of the matrix in Eq. (3) correspond to the energies of the $N+1$ exciton-polariton modes $|i\rangle$, which are eigenstates of the Hamiltonian expressed by Eq. (4). Thus, we can write:

$$\mathcal{H}|i\rangle = \sum_k \hbar \lambda_k \hat{\rho}_k^+ \hat{\rho}_k |i\rangle = \hbar \lambda_i |i\rangle, \quad (6)$$

Coefficients a_{0k} ($a_{1k}, a_{2k}, \dots, a_{Nk}$) are the weight coefficients of the exciton (cavity modes) in the polaritonic modes. The squares of the coefficients standing next to the exciton creation operator in the polariton state creation operator, i.e. $|a_{0k}|^2$, are the excitonic contribution to the polaritonic state. The energy distribution of the excitonic contribution to the polaritonic state is correlated with luminescence peaks.

3. Modelling of cavity modes

Eigenmodes for 2D meso-cavities have been studied using simulations in the “Electromagnetic Waves, Frequency Domain” module of COMSOL multiphysics software. The full size of the model is $10.2 \mu\text{m} \times 10.2 \mu\text{m}$. The geometry of the 2D meso-cavities chosen for the simulations was following: (i) the ideal square with a side of $4 \mu\text{m}$, (ii) the ideal hexagon with a side of $2 \mu\text{m}$, (iii) the ideal triangular with a side of $4.9 \mu\text{m}$, and (iv) the ideal round resonator with a radius of $2.0 \mu\text{m}$. We have chosen a resonator material with a refractive index of $n_{\text{cavity}} = 3$ and we have assumed that there is no absorption. The ambient media has a refractive index of $n_{\text{media}} = 1$. The boundaries of the model consist of an artificial absorption layer called the “Perfectly Matched Layer” (PML) to simulate open boundaries for wave equations. Perfect magnetic conductor (PMC) boundary conditions have been applied on the perimeter of the model. The mesa-cavities geometry is depicted in Fig. 1. In the model, we have used a free triangular mesh with the maximum cell size of 24 nm and 72 nm for the mesa-cavity and for the ambient media, respectively. Multifrontal massively parallel sparse direct solver (MUMPS) was used as an eigenvalue solver. The energy range for searching eigenmodes of the mesa-cavities was from 3 eV to 4 eV .

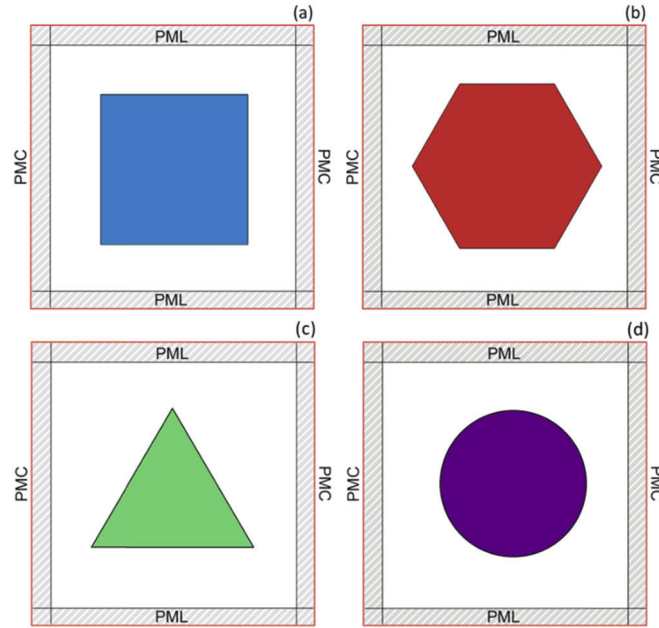


Fig. 1. Model geometry used in the simulations. (a) the model for ideal square mesa-cavity, (b) the model for ideal hexagonal mesa-cavity, (c) the model for ideal triangular mesa-cavity, (d) the model for ideal circular mesa-cavity.

4. Results and discussion

We demonstrate the theory of coupling between an exciton and several optical modes for ideal square, hexagonal, triangular and round mesa-cavities. At first, we calculated cavity mode energies, their Q-factors, and spatial distribution of the cavity modes field by solving Maxwell's equations using numerical calculations [31]. We note that the size of these cavities was chosen to be equal to several wavelengths. The modes have a different spatial distribution of the intensity of the light wave and different Q-factors. The results of simulation are shown in Figs. 2, 3, 4 and 5 for mesa-cavities of different shapes.

Examples of electromagnetic field distribution for strong localized modes calculated for the square, for the hexagonal, for the triangular, and for the round mesa-cavities are shown in Figs. 2(a), 3(a), 4(a) and 5(a), respectively. Strongly localized modes experience almost complete internal reflection at the edges of the mesa-cavity. It is clearly seen from these figures that there are areas where the maximum intensity of the standing electromagnetic wave is localized to local spots. On the contrary, weakly localized modes have a more uniform distribution of the intensity of electromagnetic field inside the mesa-cavities as illustrated in Figs. 2(b), 3(b), 4(b) and 5(b) for models with different geometries. The energies of shown modes are indicated in figure captions.

Purcell coefficient F , describing the strength of interaction of the cavity modes with an emitter reads as:

$$F_k = \frac{3}{4\pi^2} \left(\frac{\lambda_k}{n} \right)^3 \frac{Q_k}{V}, \quad (7)$$

where Q_k is the quality factor for mode k , λ_k is the wavelength of light corresponding to the frequency of the mode, n is refractive index and V is the volume of the mode [32]. For 2D case

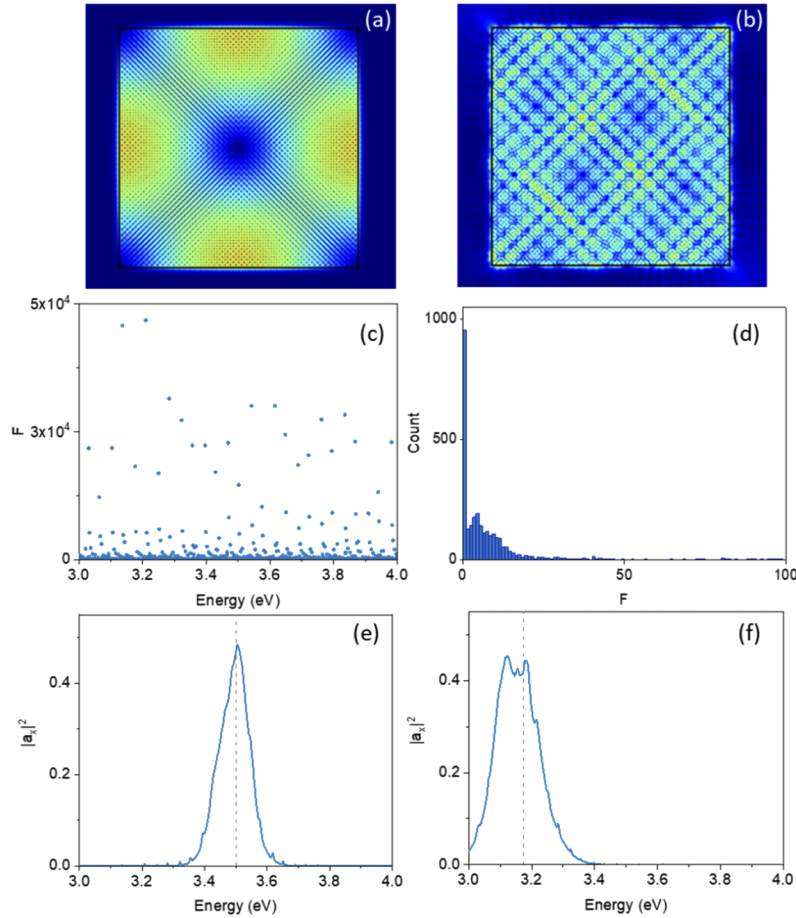


Fig. 2. (a-b): The distribution of the electromagnetic field intensity of the modes inside the ideal square resonator with a side of $4\ \mu\text{m}$ and refractive index of $n = 3$, calculated using COMSOL. (1a) Example of a strong localized mode with energy of $3.21\ \text{eV}$, and $Q = 4.6 \cdot 10^7$, (b) Example of a weakly localized mode ($3.69\ \text{eV}$, $Q = 2.1 \cdot 10^4$). Surface: Electric field (V/m). (c) Energy distribution of quantities F for the modes localized in the square, (d) Histograms illustrating distribution of cavity modes depending on the quantity F . (e-f): Dependence of the excitonic contribution to the polaritonic state $|a_{0k}|^2$ as a function of the energy of the polariton mode for a square mesa-cavity. (e) Exciton energy ($w_0 = 3.5\ \text{eV}$) is located at the distance from the mode energy with a high F . (f) Exciton energy ($w_0 = 3.173\ \text{eV}$) is located nearby to the modes energy with a high F .

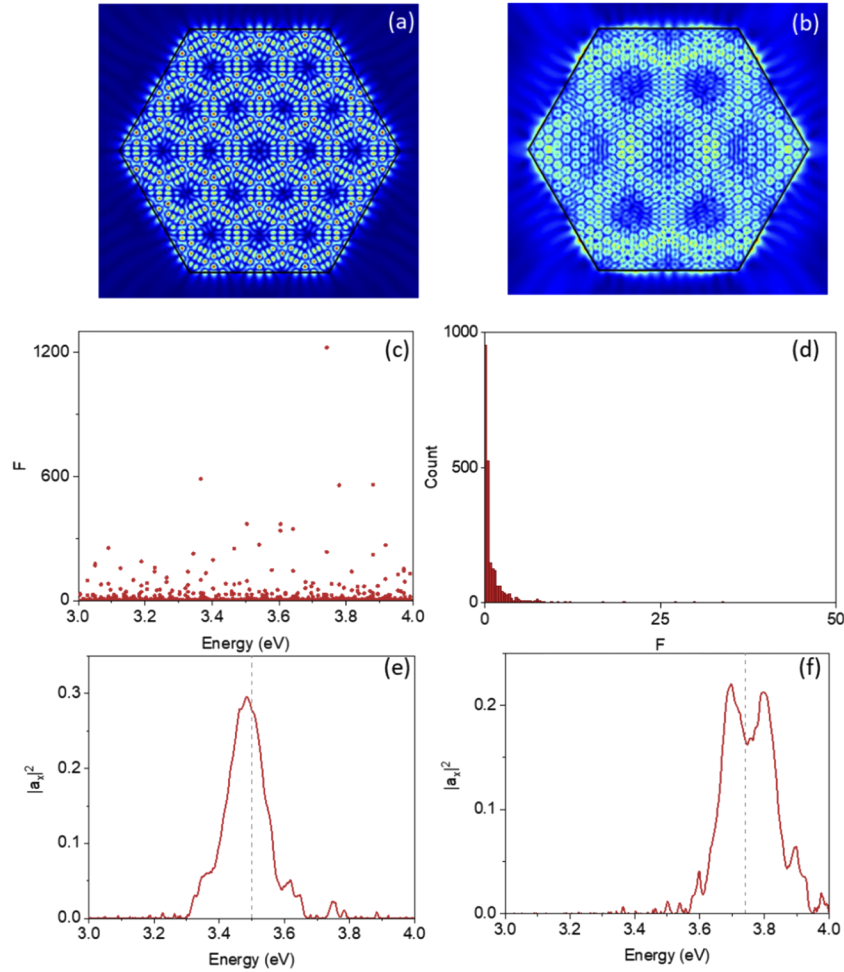


Fig. 3. (a-b): The distribution of the electromagnetic field intensity of the modes inside the ideal hexagonal resonator with a side of $2\ \mu\text{m}$ and refractive index of $n = 3$, calculated using COMSOL. (a) Example of a strong localized mode ($3.2\ \text{eV}$, $Q = 5.2 \cdot 10^4$), (b) Example of a weakly localized mode ($3.21\ \text{eV}$, $Q = 2.3 \cdot 10^3$). Surface: Electric field (V/m). (c) Energy distribution of quantities F for the modes localized in the hexagon, (d) Histograms illustrating distribution of cavity modes depending on the quantity F . (e-f): Dependence of the excitonic contribution to the polaritonic state $|a_{0k}|^2$ as a function of the energy of the polariton mode for hexagonal mesa-cavity. (e) Exciton energy ($w_0 = 3.5\ \text{eV}$) is located at the distance from the mode energy with a high F . (f) Exciton energy ($w_0 = 3.74\ \text{eV}$) is located nearby to the mode energy with a high F .

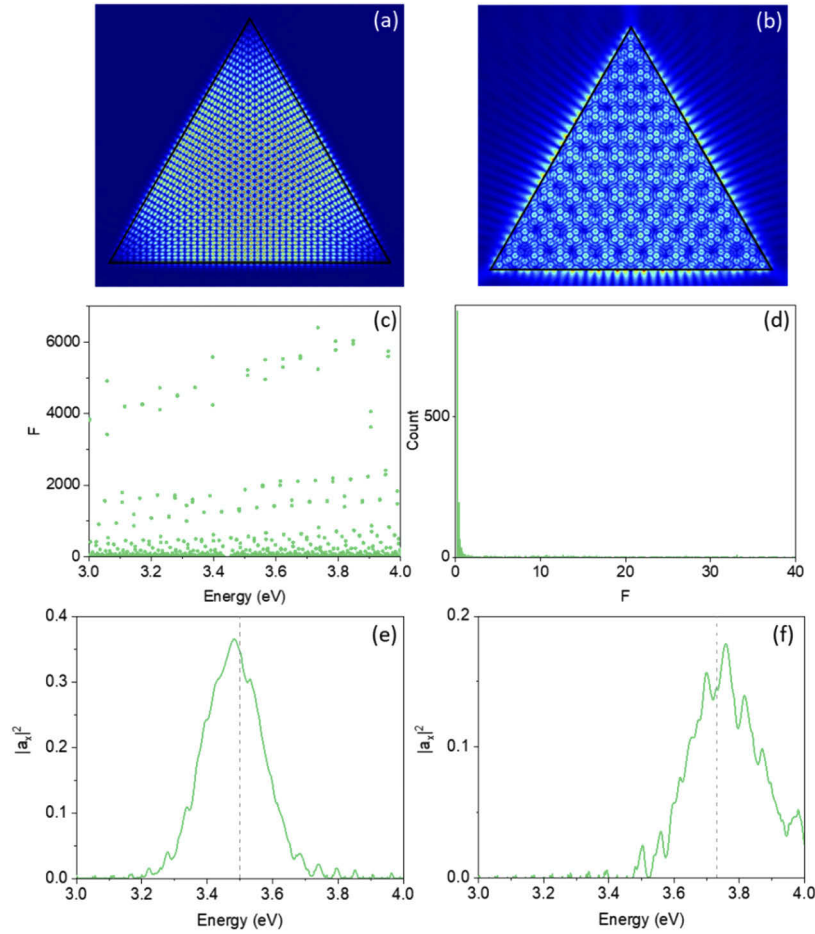


Fig. 4. (a-b): The distribution of the electromagnetic field intensity of the modes inside the ideal triangular resonator with a side of $4.9 \mu\text{m}$ and refractive index of $n = 3$, calculated using COMSOL. (a) Example of a strong localized mode (3.73 eV , $Q = 4 \cdot 10^3$), (b) Example of a weakly localized mode (3.731 eV , $Q = 6 \cdot 10^2$). Surface: Electric field (V/m). (c) Energy distribution of quantities F for the modes localized in the triangular mesa-cavity, (d) Histograms illustrating distribution of cavity modes depending on the quantity F . (e-f): Dependence of the excitonic contribution to the polaritonic state $|a_0|^2$ as a function of the energy of the polariton mode for triangular mesa-cavity. (e) Exciton energy ($w_0 = 3.5 \text{ eV}$) is located at the distance from the mode energy with a high F . (f) Exciton energy ($w_0 = 3.73 \text{ eV}$) is located nearby to the modes energy with a high F .

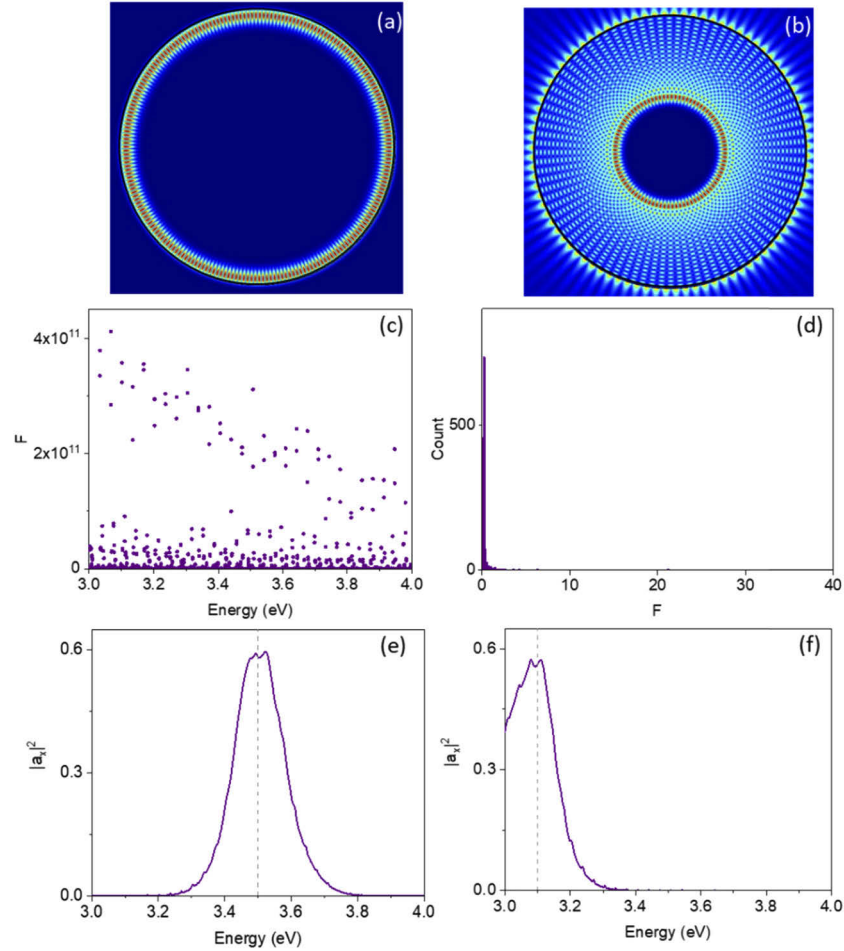


Fig. 5. (a-b): The distribution of the electromagnetic field intensity of the modes inside the ideal circular resonator with a radius of $2.0 \mu\text{m}$ and refractive index of $n = 3$, calculated using COMSOL. (a) Example of a strong localized mode (3.81 eV , $Q = 5 \cdot 10^{11}$), (b) Example of a weakly localized mode (3.812 eV , $Q = 4.6 \cdot 10^3$). Surface: Electric field (v/m). (c) Energy distribution of quantities F for the modes localized in the circle, (d) Histograms illustrating distribution of cavity modes depending on the quantity F . (e-f): Dependence of the excitonic contribution to the polaritonic state $|a_{0k}|^2$ as a function of the energy of the polariton mode for circular mesa-cavity. (e) Exciton energy ($w_0 = 3.5 \text{ eV}$) is located at the distance from the mode energy with a high F . (f) Exciton energy ($w_0 = 3.1 \text{ eV}$) is located nearby to the mode energy with a high F .

we have calculated the quantity F , defined as

$$F_k = \left(\frac{\lambda_k}{n} \right)^2 \frac{Q_k}{S}. \quad (8)$$

Figures 2(c), 3(c), 4(c) and 5(c) shows the energies and quantities F_k obtained for eigenmodes localized in the ideal square, hexagonal, triangular and round mesa-cavities, respectively. For the considered square structure, almost all modes are characterized by a very high value of F_k (about 40000). The highest F_k values have been found for the modes with energy ~ 3.2 eV. For the hexagonal structure, the quantities F_k are much lower (about 600). There is one highly localized mode at about 3.7 eV. For the triangular structure, almost all modes are characterized by the value of F_k not exceeding 6200. Highest F_k value was obtained for the mode at ~ 3.73 eV. For the round structure, almost all modes are characterized by the very high values of F_k (about 10^{11}). Figures 2(d), 3(d), 4(d) and 5(d) show the histograms illustrating distribution of cavity modes depending on the quantity F_k . Histograms show that there is a small probability of the appearance of modes with a high value of F_k for all types of resonators. Most modes are characterized by a small Purcell coefficient F_k , while a limited number of isolated cavity modes have large F_k values and can efficiently interact with the bulk exciton in these meso-cavities.

The probability that the system will emit a photon with energy $\hbar\omega_k$ and undergo transition from the state $|1, n_k\rangle$ to $|0, n_k + 1\rangle$ per unit time is determined by the Fermi golden rule:

$$W_{1 \rightarrow 0, k} = \frac{2\pi}{\hbar} |\langle 1, n_k | \hbar(g_k \hat{c}_k \hat{x}^+ + g_k^* \hat{c}_k^+ \hat{x}) | 0, n_k + 1 \rangle|^2 \rho(w_k) \quad (9)$$

where $|1, n_k\rangle$ is the excited state and the field has n_k photons in mode k , $|0, n_k + 1\rangle$ is the ground state and the field has $n_k + 1$ photons in mode k . $\rho(w_k)$ is the energy density of the number of final states of the system. The interaction force of an exciton with a certain mode g_k is determined from Eq. (9) as:

$$|g_k| = \sqrt{\frac{W_{1 \rightarrow 0, k}^0 F_k}{2\pi \hbar (n_k + 1) \rho(\hbar\omega_k)}}, \quad (10)$$

where $W_{1 \rightarrow 0, k}^0$ is the probability of excitonic emission in the uniform media.

Now, using the known values of the energies and coupling constants, we can find the excitonic contribution to the polaritonic state. Figures 2(e)–2(f), 3(e)–3(f), 4(e)–4(f) and 5(e)–5(f) illustrate spectral dependence of the excitonic contribution to the polaritonic state for the square, hexagonal, triangular and round mesa-cavities, respectively. The exciton emission spectrum of the cavity observed in the experiments is defined by the spectral dependence of the Hopfield coefficients and the occupancy of polariton states determined by the pumping of the cavity and the relaxation of polaritons [33]. Here we focus on the mode spectrum of exciton-polaritons in microcavities, although a more precise description of the emission spectrum of the system can be developed within the framework of the approach based on a density matrix with Lindblad terms, where the pumping and damping rates are also taken into account [34].

In Figs. 2(e), 3(e), 4(e) and 5(e), the exciton energy is located at the distance from the mode energy with a high F . The exciton energy for the square, the hexagon, the triangular and the circle is equal to 3.5 eV. In all cases, the shape of the distribution of the exciton contribution looks like a single peak, which is slightly shifted from the original exciton energy. In Figs. 2(f), 3(f), 4(f) and 5(f), the exciton energy is located nearby to the mode energy with a high F , and is equal to 3.173 eV, 3.74 eV, 3.73 eV and 3.1 eV for the square, the hexagon, the triangular and the circle, respectively. These energies correspond to regions where the eigenmodes of the structures have the highest value of the Purcell factor.

For the hexagonal cavity, two pronounced peaks are visible in graph in Fig. 3(f). The distance between the peaks is 100 meV. For a square cavity, in Fig. 2(f), three weakly pronounced peaks

are visible. The distance between the peaks is approximately 30 meV. For a triangular and round cavity, in Figs. 4(f) and 5(f), respectively, only one pronounced peak is visible, with small inhomogeneities. This behaviour of the exciton contributions is obviously characterized by the presence of isolated eigenmodes with a high Purcell factor in the structure. Thus, for the hexagonal structure, where there is only one mode with a relatively high value of the Purcell factor, a typical Rabi splitting is observed. For a square structure, where there are already two pronounced modes with a relatively high value of the Purcell factor, the splitting is much weaker.

Since the mode distribution depends on the shape of the structure, it can be observed that for shapes with a large number of angles, the probability of the appearance of one isolated mode with a high value of the Purcell factor and correspondingly pronounced splitting of the peaks in the spectrum increases.

5. Summary

The spectrum of the optical modes has been calculated in meso-cavities (i.e. the cavities whose size corresponds to few dozens of wavelengths) with triangular, square, hexagonal and cylindrical shapes. We have shown that in such types of the structures neighbouring modes could have Q-factors, which differ by orders in magnitudes. There is a small probability of the appearance of modes with a high value of Q-factor for all types of resonators and such modes interacts with excitons more efficiently than the modes with small Q-factors.

The Hamiltonian describing the interaction of cavity and exciton modes in such structures has been obtained, the spectrum of the Hopfield coefficients of polaritonic modes was constructed and a set of polariton modes was obtained. Analysis of the spectrum of the Hopfield coefficients demonstrates that in meso-cavities, the interaction of exciton and photon modes can occur in both weak and strong coupling regime despite a high density of cavity modes caused by the large size of the systems.

Funding

Russian Science Foundation (16-12-10503); Vetenskapsrådet (2019-05154); Energimyndigheten (46563-1).

Disclosures

The authors declare no conflicts of interest.

References

1. C. Weisbuch, M. Nishioka, A. Ishikawa, and Y. Akarawa, "Observation of the coupled exciton-photon mode splitting in a semiconductor quantum microcavity," *Phys. Rev. Lett.* **69**(23), 3314–3317 (1992).
2. R. Houdre, R. P. Stanley, U. Oesterle, M. Illegems, and C. Weisbuch, "Room temperature exciton-photon Rabi splitting in a semiconductor microcavity," *J. Phys. IV* **3**(C5), 51–58 (1993).
3. I. Abram and J. L. Oudar, "Spontaneous emission in planar semiconductor microcavities displaying vacuum Rabi splitting," *Phys. Rev. A* **51**(5), 4116–4122 (1995).
4. S. Pau, G. Björk, J. Jacobson, H. Cao, and Y. Yamamoto, "Microcavity exciton-polariton splitting in the linear regime," *Phys. Rev. B* **51**(20), 14437–14447 (1995).
5. T. A. Fisher, A. M. Afshar, D. M. Whittaker, M. S. Skolnick, J. S. Roberts, G. Hill, and M. A. Pate, "Electric-field and temperature tuning of exciton-photon coupling in quantum microcavity structures," *Phys. Rev. B* **51**(4), 2600–2603 (1995).
6. G. Panzarini, L. C. Andreani, A. Armitage, D. Baxter, M. S. Skolnick, V. N. Astratov, M. R. Vladimirova, and M. A. Kaliteevski, "Exciton-light coupling in single and coupled semiconductor microcavities: Polariton dispersion and polarization splitting," *Phys. Rev. B* **59**(7), 5082–5089 (1999).
7. M. A. Kaliteevski, S. Brand, R. A. Abram, A. V. Kavokin, and L. S. Dang, "Whispering gallery polaritons in cylindrical cavities," *Phys. Rev. B* **75**(23), 233309 (2007).
8. D. Gerace and L. C. Andreani, "Quantum theory of exciton-photon coupling in photonic crystal slabs with embedded quantum wells," *Phys. Rev. B* **75**(23), 235325 (2007).

9. D. M. Whittaker, P. S. S. Guimaraes, D. Sanvitto, H. Vinck, S. Lam, A. Daraei, J. A. Timpson, A. M. Fox, M. S. Skolnick, Y.-L. D. Ho, J. G. Rarity, M. Hopkinson, and A. Tahraoui, "High Q modes in elliptical microcavity pillars," *Appl. Phys. Lett.* **90**(16), 161105 (2007).
10. J. Hendrickson, B. C. Richards, J. Sweet, G. Khitrova, A. N. Poddubny, E. L. Ivchenko, M. Wegener, and H. M. Gibbs, "Excitonic polaritons in Fibonacci quasicrystals," *Opt. Express* **16**(20), 15382–15387 (2008).
11. D. Bajoni, D. Gerace, M. Galli, J. Bloch, R. Braive, I. Sagnes, A. Miard, A. Lemaitre, M. Patrini, and L. C. Andreani, "Exciton polaritons in two-dimensional photonic crystals," *Phys. Rev. B* **80**(20), 201308 (2009).
12. B. Piętko, D. Zygmunt, M. Król, M. R. Molas, A. A. L. Nicolet, F. Morier-Genoud, J. Szczytko, J. Lusakowski, P. Zieba, I. Tralle, P. Stepnicki, M. Matuszewski, M. Potemski, and B. Deveaud, "Magnetic field tuning of exciton-polaritons in a semiconductor microcavity," *Phys. Rev. B* **91**(7), 075309 (2015).
13. T. Q. P. Vuong, G. Cassaboïs, P. Valvin, S. Liu, J. H. Edgar, and B. Gil, "Exciton-phonon interaction in the strong-coupling regime in hexagonal boron nitride," *Phys. Rev. B* **95**(20), 201202 (2017).
14. C. Schneider, J. Fischer, M. Amthor, S. Brodbeck, I. G. Savenko, I. A. Shelykh, A. Chernenko, A. Rahimi-Iman, V. D. Kulakovskii, S. Reitzenstein, N. Y. Kim, M. Durnev, A. V. Kavokin, Y. Yamamoto, A. Forchel, M. Kamp, and S. Höfling, "Exciton-polariton lasers in magnetic fields," *Proc. SPIE* **8993**, 899308 (2014).
15. G. Shan, X. Zhao, and W. Huang, "Nanolaser with a single-graphene-nanoribbon in a microcavity," *J. Nanoelectron. Optoelectron.* **6**(2), 138–143 (2011).
16. V. K. Kalevich, M. M. Afanasiev, V. A. Lukoshkin, D. D. Solnyshkov, G. Malpuech, K. V. Kavokin, S. I. Tsintzos, Z. Hatzopoulos, P. G. Savvidis, and A. V. Kavokin, "Controllable structuring of exciton-polariton condensates in cylindrical pillar microcavities," *Phys. Rev. B* **91**(4), 045305 (2015).
17. C. E. Platts, M. A. Kaliteevski, S. Brand, R. A. Abram, and A. V. Kavokin, "Whispering-gallery polaritons in nanospheres," *Phys. Rev. B* **79**(24), 245322 (2009).
18. R. Jia, D. S. Jiang, P. H. Tan, and B. Q. Sun, "Quantum dots in glass spherical microcavity," *Appl. Phys. Lett.* **79**(2), 153–155 (2001).
19. B. L. Altshuler, A. G. Aronov, and P. A. Lee, "Interaction effects in disordered Fermi systems in two dimensions," *Phys. Rev. Lett.* **44**(19), 1288–1291 (1980).
20. M. Koch, F. Ample, C. Joachim, and L. Grill, "Voltage-dependent conductance of a single graphene nanoribbon," *Nat. Nanotechnol.* **7**(11), 713–717 (2012).
21. R. A. Jalabert, H. U. Baranger, and A. D. Stone, "Conductance fluctuations in the ballistic regime: A probe of quantum chaos?" *Phys. Rev. Lett.* **65**(19), 2442–2445 (1990).
22. Y. Aharonov and D. Bohm, "Significance of electromagnetic potentials in quantum theory," *Phys. Rev.* **115**(3), 485–491 (1959).
23. Q.-Y. Lu, X.-H. Chen, W.-H. Guo, L.-J. Yu, Y.-Z. Huang, J. Wang, and Y. Luo, "Mode characteristics of semiconductor equilateral triangle microcavities with side length of 5–20 μm ," *IEEE Photon. Technol. Lett.* **16**(2), 359–361 (2004).
24. T.-C. Chang, K.-B. Hong, Y.-Y. Lai, Y.-H. Chou, S.-C. Wang, and T.-C. Lu, "ZnO-Based Microcavities Sculpted by Focus Ion Beam Milling," *Nanoscale Res. Lett.* **11**(1), 319 (2016).
25. G. Yuan, C. Zhang, K. Xiong, and J. Han, "InGaN/GaN microdisks enabled by nanoporous GaN cladding," *Opt. Lett.* **43**(22), 5567–5570 (2018).
26. S. L. McCall, A. F. J. Levi, R. E. Slusher, S. J. Pearton, and R. A. Logan, "Whispering-gallery mode microdisk lasers," *Appl. Phys. Lett.* **60**(3), 289–291 (1992).
27. T. V. Shubina, G. Pozina, V. N. Jmerik, V. Y. Davydov, C. Hemmingsson, A. V. Andrianov, D. R. Kazanov, and S. V. Ivanov, "III-nitride tunable cup-cavities supporting quasi whispering gallery modes from ultraviolet to infrared," *Sci. Rep.* **5**(1), 17970 (2016).
28. G. Pozina, A. R. Gubaydullin, M. I. Mitrofanov, M. A. Kaliteevski, I. V. Levitskii, G. V. Voznyuk, E. E. Tatarinov, V. P. Evtikhiev, S. N. Rodin, V. N. Kaliteevskiy, and L. S. Chechurin, "Approach to high quality GaN lateral nanowires and planar cavities fabricated by focused ion beam and metal-organic vapor phase epitaxy," *Sci. Rep.* **8**(1), 7218 (2018).
29. G. Pozina, C. Hemmingsson, A. V. Belonovskii, I. V. Levitskii, M. I. Mitrofanov, E. I. Girshova, K. A. Ivanov, S. N. Rodin, K. M. Morozov, V. P. Evtikhiev, and M. A. Kaliteevski, "Emission properties of GaN planar hexagonal microcavities," *Phys. Status Solidi A* 1900894 (2019).
30. R. Loudon, "Quantum Theory of Light," (Oxford University, 2000), pp. 276.
31. Modeling of the cavity modes in structure was made using COMSOL Multiphysics software.
32. E. M. Purcell, H. C. Torrey, and R. V. Pound, "Resonance absorption by nuclear magnetic moments in a solid," *Phys. Rev.* **69**(1–2), 37–38 (1946).
33. E. Tokunaga, A. L. Ivanov, S. V. Nair, and Y. Masumoto, "Hopfield coefficients measured by inverse polariton series," *Phys. Rev. B* **63**(23), 233203 (2001).
34. F. P. Laussy, E. del Valle, and C. Tejedor, "Luminescence spectra of quantum dots in microcavities. I. Bosons," *Phys. Rev. B* **79**(23), 235325 (2009).